Journal of Statistical Physics, Vol. 98, Nos. 3/4, 2000

Conductance and Statistical Properties of Chaotic and Integrable Electron Waveguides

Gursoy B. Akguc[1] and L. E. Reichl[1]

Received May 4, 1999; final September 30, 1999

We show that the S-matrix for electrons propagating in a waveguide has different statistical properties depending on whether the waveguide cavity shape gives rise to chaotic or integrable behavior classically. We obtain distributions of energy level spacings for integrable and chaotic billiards shaped like the waveguide cavity. We also obtain distributions for Wigner delay times and resonance widths for the waveguide, for integrable and chaotic cavity geometries. Our results, obtained by direct numerical calculation of the electron wave function, are consistent with the predictions of random matrix theory.

KEY WORDS: Conductance; electron waveguide; electron scattering; random matrix theory; finite element method.

1. INTRODUCTION

In recent years it has become possible experimentally to produce two dimensional micron size electron waveguides at semiconductor interfaces. The electron dynamics in these devices is two dimensional because the degree of freedom perpendicular to the interface allows only a single quantum eigenstate. The shape of the confining walls can strongly affect the qualitative nature of the electron transmission probability and, in experiments, geometries have been[(1)] selected specifically to show this aspect of electron conductance. The transmission properties of a waveguide whose classical counterpart exhibits chaotic scattering will be different from one which is classically integrable.[(2)] This difference between classically chaotic

[1] Center for Studies in Statistical Mechanics and Complex Systems The University of Texas at Austin, Austin, Texas 78712.

0022-4715/00/0200-0813$18.00/0

and classically regular quantum systems also occurs for closed systems.[3] For example, for closed systems it has been shown that the quantum counterpart of a classically chaotic system has a different eigenvalue distribution compared to eigenvalue distributions obtained for classically integrable geometries.[4]

Quantum chaotic scattering in 2-dimensional electron waveguides has been an important research topic in recent years due to its practical importance and rich theoretical implications.[5] The direct solution of the Schrödinger equation for a 2-dimensional electron gas can be obtained numerically for an open system (the scattering case). However, it is difficult to obtain solutions in regimes with many propagating modes due to necessity of having more mesh points to resolve the wave function in the scattering region. Statistical (random matrix theory)[6–8] and semi-classical methods[5, 9, 10] are the main theoretical tools used to describe chaotic behavior in complex geometries with many propagating modes.

In this paper, we numerically solve the Schrödinger equation for the electron wave function in electron waveguides with both chaotic and regular geometries. We have chosen a waveguide with straight leads and with a cavity which is basically rectangular but has one rippled wall with a ripple amplitude which can be varied. We focus on an energy interval where only four propagating modes occur in the leads. This regime contains enough modes to enable us to build statistics, but yet it is far from the semi-classical regime. As we shall show, the statistical properties of the transmission probability are quite different for the case of zero ripple amplitude and for the case of large ripple amplitude.

The waveguide we consider in this paper is shown in Fig. 1. We attach two aligned leads, each of width $w = 100$ Å, to a rippled box. Since such waveguides can be fabricated in GaAs–AlGaAs heterostructures, we assume the electrons have an effective mass $m^* = 0.067\, m_e$, where m_e is the mass of the electron. The typical electron density is $n_s = 2.8 \cdot 10^{15}\ \mathrm{m}^{-2}$ and the Fermi energy is $E_F = \pi h^2 n_s / m^* = 10$ mev. In this paper, we have neglected electron–electron interactions in order to compare our numerical results to random matrix predictions which also neglect electron–electron interactions.

In the following sections, we compare the scattering properties of two different waveguides, one with a rectangular cavity and the other with a rippled wall whose ripple amplitude is large enough so that the motion inside is completely chaotic. We begin in Section 2 by comparing the energy eigenvalue spacing statistics of a particle in closed billiards with these shapes. In Section 3, we analyze the spectral properties of the scattering S-matrix for waveguides with both rectangular and rippled cavities. In the last section, we make some concluding remarks.

2. CLOSED SYSTEM

A closed ripple billiard can be visualized in Fig. 1 if we remove the leads and put hard walls along the dotted lines. The ripple boundary has the form, $y = b + a \cdot \cos((4\pi/L)\, x)$ and we have chosen the following parameters for the rippled box, $L = 200$ Å, $d = 200$, and $a = 3, 5, 7, 9, 10$ Å. We obtain data for this range of ripple amplitudes in order to improve the statistics for our histograms. A Poincare surface of section (obtained using the Birkhoff coordinates on the lower boundary) shows that motion of a classical particle is fully chaotic for ripple size $a > 2$ Å and it is integrable when $a = 0$ Å. For the closed system, the Schrödinger equation, $-(h^2/2m)(\partial_x^2 + \partial_y^2)\, \psi = E_n \psi$, is subject to Dirichlet boundary conditions on all the walls. The wave function ψ is real with real energy eigenvalues E_n. We have obtained the energy eigenvalues for the rectangular and ripple billiards in two different ways, one by direct diagonalization of the Hamiltonian matrix and the other using the finite element program that we use to study the electron waveguides. This gives us one way to check our finite element waveguide program. For the rectangular billiard the eigenvalues are known and can be written in analytic form, which we give below. For the chaotic billiard, we have diagonalized the Hamiltonian matrix using a method that was used for an infinite ripple channel.[11] This method is interesting in its own right and we describe it in the Appendix.

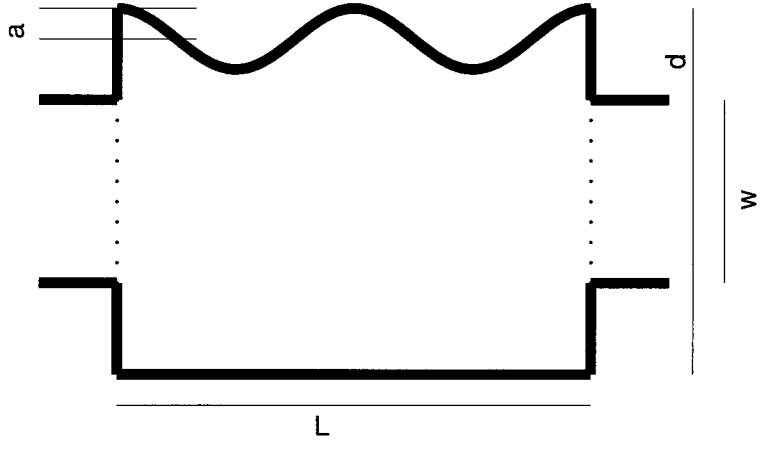

Fig. 1. The geometry of the two dimensional electron wave guide used in our calculations. The rippled billiard is the region defined with dotted lines replaced by walls and leads removed. Here "a" is the width of the ripple, "d = b + a" is the width of the cavity, "w" is the width of the leads, and "L" is the length of the cavity.

One common test of whether a bounded quantum system is integrable or chaotic is to plot a histogram of the nearest neighbor spacings between energy eigenvalues of the system. The energy eigenvalues of the rectangular billiard are given by $E_{mn} = (m\pi/d)^2 + (n\pi/L)^2$, where m and n are integers and we have chosen $d = 199$ Å and $L = 200$ Å. In Fig. (2.a), we show the distribution of spacings between nearest neighbor energy eigenvalues (obtained from the analytic expression above) for the rectangular billiard using 2500 eigenvalue spacings. In Fig. (2.b), we show the histogram of nearest neighbor energy eigenvalue spacings for the ripple billiard with $a = 10$ Å, using 3000 eigenvalue spacings obtained using the techniques described in the Appendix. In both cases, we have separated states of different parity and we have found energy spacings only for states of the same parity. For each value of parity, we have unfolded the energy eigenvalues so that we have a unit average spacing over any energy interval[22] The nearest neighbor energy eigenvalue spacing distribution for the rectangular billiard is known to be Poisson,[7] and that is what we find for our system.

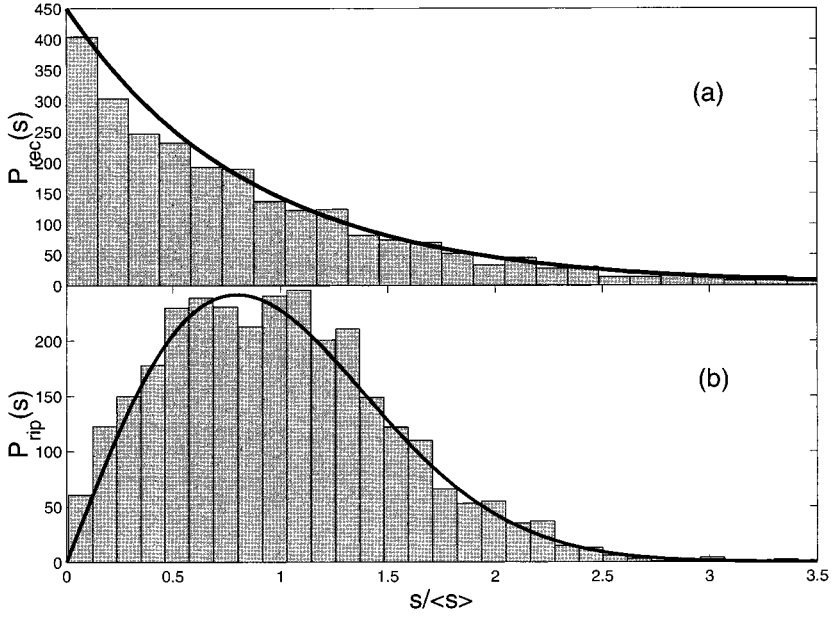

Fig. 2. Histogram of nearest-neighbor eigenvalue spacings in terms of scaled spacing for (a) rectangular box, (b) Rippled box. In (a) we have chosen $L = 199$ Å and $d = 200$ Å with 2500 eigenvalues. The fitting curve is $y = \exp(-s/\langle s \rangle)$. In (b) we have used 3000 eigenvalues for the ripple size $a = 10$ Å. The fitting curve is the Wigner distribution with unit average spacing.

The nearest-neighbor spacing for the ripple billiard resembles the Wigner distribution

$$P_{\text{Wigner}}(s) = \frac{\pi}{2} s \exp\left(-\frac{\pi}{4} s^2\right) \tag{1}$$

which is the predicted result of random matrix theory[7] for a closed quantum system whose underlying dynamics is chaotic.

Let us note that we have obtained good agreement using the same finite element method (FEM)[13] that we will use for the open systems in the remainder of the paper. For the integrable case, the FEM agrees with exact results to an accuracy of 10^{-6}, and the diagonalization technique (see Appendix) agrees to an accuracy of 10^{-12}. For the chaotic case, the FEM agrees with the diagonalization method to an accuracy of 10^{-4}. The FEM leads to a generalized eigenvalue problem for the rippled box.

3. THE OPEN SYSTEM

3.1. Chaotic Versus Integrable Wave Guide

Two infinitely long leads can be attached to the rippled billiard to convert the system into an electron waveguide (an open system). The Schrödinger equation describes the motion of the electron wave function inside the waveguide. We assume the potential is zero inside the cavity and inside the leads and infinite outside these regions (the walls are infinitely hard). The wave function inside the cavity vanishes at the boundary of the cavity. The remaining boundary conditions are given in terms of the continuity condition for the wave function at the cavity-lead boundary. The solution of the Schrödinger equation inside the leads is known and is given as a superposition of plane waves,

$$\begin{aligned} \psi^L(x, y) &= \sum_{n=1}^{N} (a_n^L e^{ik_n x} + b_n^L e^{-ik_n x})\, \phi_n(y) \qquad \text{for} \quad x \leqslant 0 \\ \psi^R(x, y) &= \sum_{n=1}^{N} (a_n^R e^{ik_n x} + b_n^R e^{-ik_n x})\, \phi_n(y) \qquad \text{for} \quad x \geqslant L \end{aligned} \tag{2}$$

where $\phi_n = \sqrt{2/w}\, \sin(n\pi y/w)$ and N is the number of transverse modes. N is infinite in principal but we have truncated it so that all propagating and some evanescent modes have been included in calculations. The particle energy is the sum of a quantized part due to the transverse degree of freedom, and a continuous part due to the longitudinal motion. It

has the form $E = h^2k_n^2/2m + E_n$, where k_n is the wave vector, $k_n = \sqrt{(2m/h^2)(E - E_n)}$, and $E_n = h^2n^2\pi^2/2md^2$ is the energy associated with the transverse motion. Boundary conditions on the cavity-lead interface are determined by the continuity of the wave function and its first derivative on the interface.

The electron probability density and current inside the cavity are given in terms of the wave function as,

$$\rho(x, y) = \psi^*(x, y)\,\psi(x, y) \tag{3}$$

$$j(x, y) = \frac{i}{2m}\left(\psi^*(x, y)\cdot\nabla\psi(x, y) - \psi(x, y)\cdot\nabla\psi^*(x, y)\right) \tag{4}$$

respectively, where ψ^* is Hermitian conjugate of ψ and $\nabla = \hat{\mathbf{x}}\partial_x + \hat{\mathbf{y}}\partial_y$.

The S-matrix for the waveguide is given in terms of the transmission probability amplitudes, $t_{mn}(E) = (\sqrt{k_n/k_m})\,a_n^R/a_m^L$, and $t'_{mn}(E) = (\sqrt{k_n/k_m})\,b_n^L/b_m^R$, and the reflection probability amplitudes, $r_{mn}(E) = (\sqrt{k_n/k_m})\,b_n^L/a_m^L$, and $r'_{mn}(E) = (\sqrt{k_n/k_m})\,a_n^R/b_m^R$. The scaling with wave vector is necessary since the transmission amplitudes are defined as the ratio of currents from one propagating mode to another. The S-matrix is given in terms of reflection and transmission matrices so that $\bar{S} \equiv \left(\begin{smallmatrix}\bar{r} & \bar{t}'\\ \bar{t} & \bar{r}'\end{smallmatrix}\right)$, The matrices, $\bar{r}$ and $\bar{r}'$, describe reflection from left to left and right to right, respectively. The matrices, $\bar{t}$ and $\bar{t}'$ describe transmission from left to right and from right to left, respectively. The total transmission and reflection probabilities for propagating mode, m, are

$$T_m = \sum_{n=1}^{N} |t_{nm}|^2 \qquad \text{and} \qquad R_m = \sum_{n=1}^{N} |r_{mn}|^2 \tag{5}$$

respectively. The Landauer conductance, G, is proportional to the sum of all transmission probabilities,

$$G = \frac{2e^2}{h}\sum_m T_m \tag{6}$$

We can define a vector of coefficients describing a wave incident on the cavity,[7]

$$\bar{c}^{\,\text{in}} \equiv (a_1^L, a_2^L, \ldots, a_N^L, b_1^R, b_2^R, \ldots, b_N^R) \tag{7}$$

A complimentary vector describing transmitted and reflected waves is defined as

$$\bar{c}^{\,\text{out}} \equiv (a_1^R, a_2^R, \ldots, a_N^R, b_1^L, b_2^L, \ldots, b_N^L) \tag{8}$$

The scattering matrix, $\bar{S}$, is a $2N \times 2N$ unitary matrix which relates these two vectors,

$$\bar{c}^{\,\text{out}} = \bar{S} \cdot \bar{c}^{\,\text{in}} \tag{9}$$

$\bar{S}$ is a unitary matrix because of current conservation and it is also symmetric due to the time reversal symmetry of our system. For the integrable cavity we have 4-fold symmetry and the $\bar{S}$ is block diagonal.[14] Eigenvalues of the S-matrix lie on the unit circle and thus they can be represented by the phase angle of the complex exponential, $e^{i\theta_n(E)}$ where the eigenphases, $\theta_n(E)$, are functions of energy (see Fig. 3). A FEM has been used to find the wave function inside the cavity. A description of this method can be found in reference.[15] (It is useful to note that this FEM method has also been used to find the distribution of resonance spacings for a Sinai billiard wave guide.[16]) Since it was necessary to have high accuracy when calculating the S-matrix we used a quadratic basis and 9393 adaptive mesh points which minimize error coming from the curved

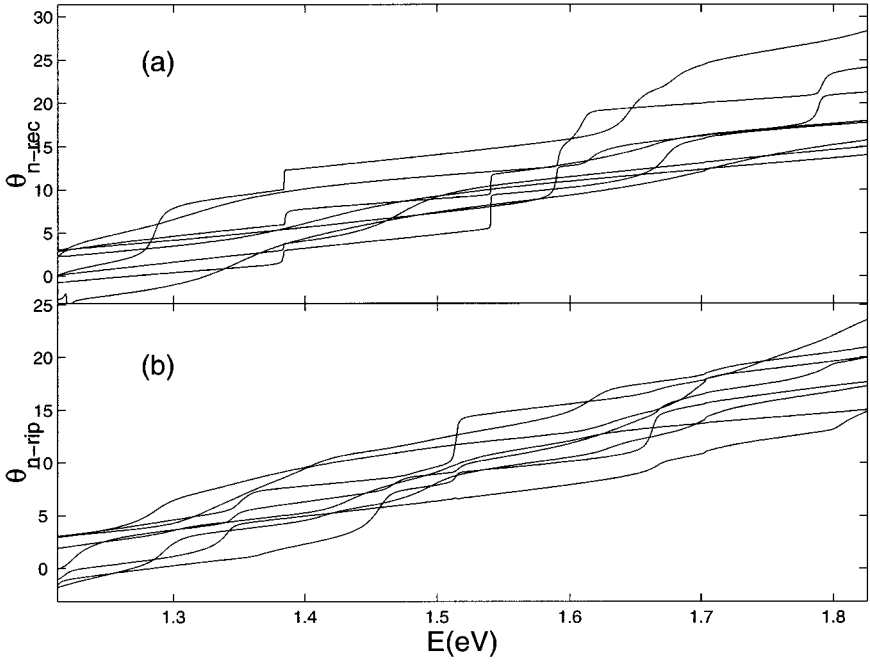

Fig. 3. Phases of S matrix. (a) Integrable waveguide, (b) ripple waveguide ($a = 10$ Å). The angle θ is in radians.

boundary condition. We checked our numerical results by requiring that the absolute value of S-matrix eigenvalues be equal to one. The error is less than 10^{-5} for the calculated eigenvalues of the S-matrix.

We find the eigenvalues of the S-matrix at each energy by diagonalizing the S-matrix for that energy. However, the eigenvalues found for neighboring energies are not ordered. Therefore, we use the following technique to order eigenvalues in energy. For each eigenvector at energy, E, we calculate its inner product with each of the eigenvectors at energy $E+\Delta E$. For each S-matrix eigenvector at energy, E, the maximum of the inner products with the eigenvectors at energy, $E+\Delta E$, identifies the corresponding eigenvector at energy, $E+\Delta E$. In Fig. 3, we show the phase angle curves in the energy interval where the lead can support 4 propagating modes. In this energy interval, the S-matrix is an 8 by 8 matrix and there are 8 eigenphases. After unwrapping phase angles ("unwrapping" means we allow the phase to grow continuously when it becomes greater than π rather than map it back onto the $[-\pi, \pi]$ interval), we obtain a continuous change in the eigenphases as a function of energy. Figure 3a shows the eigenphases for the waveguide with rectangular cavity ($a=0$ Å), and Fig. 3b shows them for the ripple cavity ($a=10$ Å). It is interesting to note that the eigenphases of the rectangular cavity undergo more abrupt changes than those of the ripple cavity. These abrupt changes can be understood in terms of the matching of transverse modes in the leads and cavities. For a rectangular cavity, the electron state inside the cavity consists of a superposition of a few transverse modes with the wave number different than the transverse mode in the leads. Only modes of like parity in the lead and cavity can couple. As energy is varied allowed modes in the cavity can abruptly change parity. If a system is at resonance for a given energy, a small change in energy can cause the system to go abruptly out of resonance as the parity of cavity modes change. For the ripple cavity, the electron state in the cavity has no definite parity and abrupt mismatch cannot occur as energy is changed. We will see these different behaviors of the rectangular and ripple cavities again when we look at the Wigner delay times.

Matrix elements and eigenvalues of the S-matrix at neighboring energies are correlated. In order to see the range of the correlation we have calculated the auto-correlation function of S-matrix eigenvalues in the following way,

$$C_s(\Delta E) \equiv \left(\frac{N}{\pi}\right)^2 \frac{1}{2N(E_1-E_2)} \sum_n^{2N} \int_{E_1}^{E_2} dE[s_n(E+\Delta E)\, s_n(E) - (s_n(E))^2] \tag{10}$$

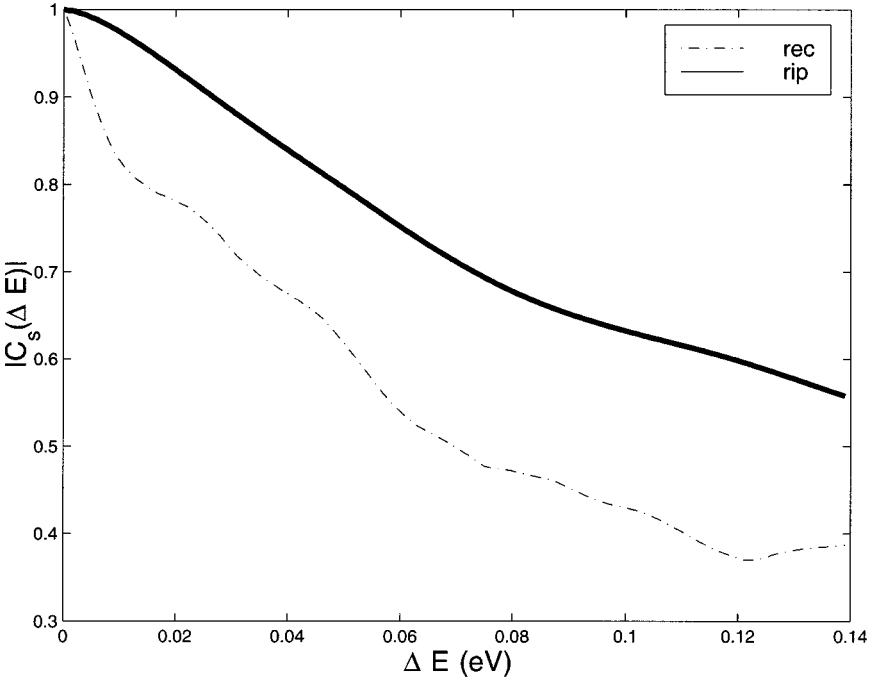

Fig. 4. The auto-correlation function of the eigenvalues of S-matrix elements averaged over the total number of eigenvalues. The absolute value of the correlation (in units of eV) is shown for $a = 10$ Å ripple (solid curve) and rectangular (dashed curve) waveguides.

where $s_n(E) = e^{i\theta_n(E)}$ are eigenvalues of the S-matrix at energy, E. The integration in Eq. (10) is approximated by a summation over energies, with energy spacings, $\delta E \approx 0.002$ eV. The absolute value of normalized correlation function, $|C_s(\Delta E)|/|C_s(0)|$, is shown in Fig. 4 for ripple ($a = 10$ Å) and integrable cavities. We see that the correlation range of the eigenvalues is greater for the chaotic waveguide than in the integrable waveguide. This is directly related to the fact that the scattering resonances are sharper (as a function of energy) for the rectangle cavity than for the ripple cavity. The correlation function in Eq. (10) has also been calculated analytically from random matrix theory in reference.[17] We say more about the comparison between our exact results and the random matrix theory predictions in a later section.

The Wigner delay time matrix, $\bar{\tau}(E)$, is defined in terms of the energy derivative of the S-matrix:

$$\bar{\tau}(E) = i\hbar \frac{\partial \bar{S}^{\dagger}}{\partial E} \bar{S} \tag{11}$$

When the S-matrix is diagonalized, the partial delay time, $\tau_n(e)$, for the nth eigenmode of the S-matrix, is given as the derivative of the nth eigenphase, $\tau_n = \partial\theta_n(E)/\partial E$. The Wigner delay time is a measure of the time delay of the electron in traversing the waveguide cavity as compared to the time it would take to travel the same distance in the leads (see ref. 18 for additional discussion). We have computed the partial Wigner delay times, as a function of energy, for both the rectangular and ripple ($a = 10$ Å) waveguides. Figures 5 and 6 show the relation between the transmission probability and the partial Wigner delay time for the two geometries. Resonances occur at energies at which the transmission probability drops toward zero and the Wigner delay time is peaked. This resonance structure comes from the fact that transmission poles and zeros occur in pairs due to the unitarity of S-matrix. (See ref. 19.) The peak values of Wigner delay time show that the delay of the electron in traversing the cavity is greatly increased at resonance energies. The first thing to note is that the integrable waveguide has a Wigner delay time at resonance energies which can be an order of magnitude larger than for the chaotic case. For example

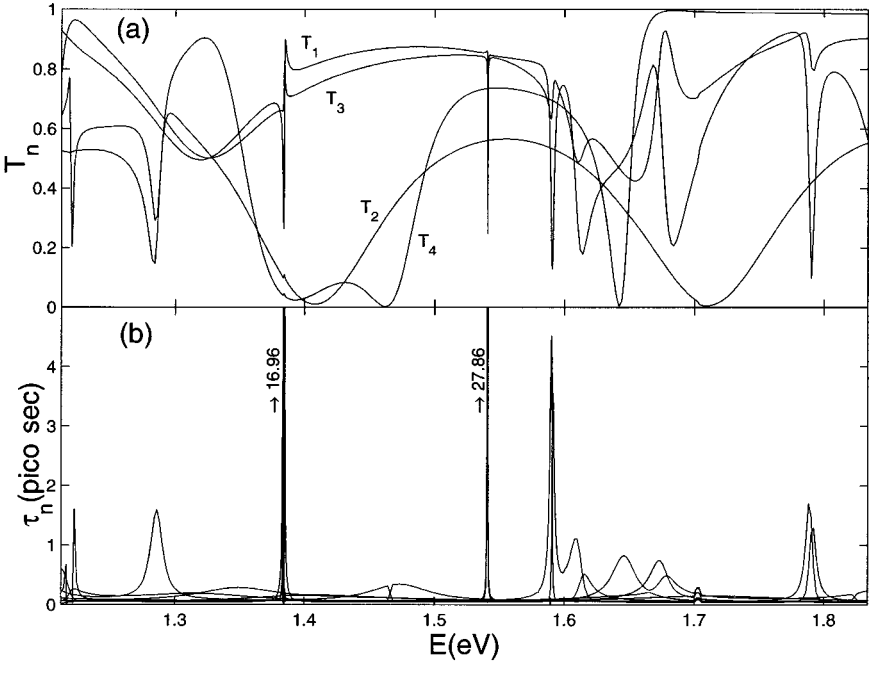

Fig. 5. (a) The transmission probability vs. energy and (b) partial Wigner delay time (in units of pico-second) vs. energy for integrable waveguide.

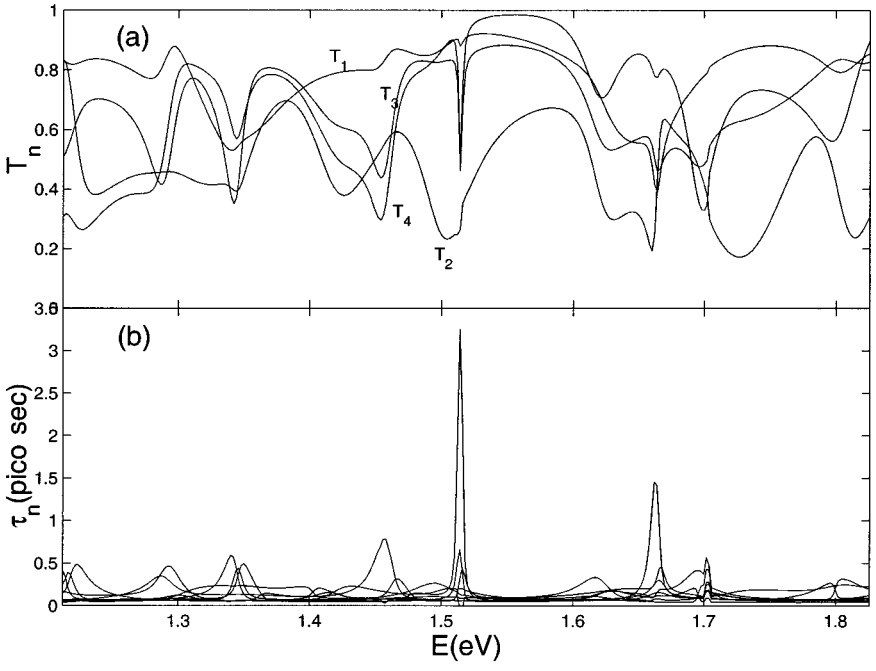

Fig. 6. (a) The transmission probability vs. energy and (b) partial Wigner delay time (in units of pico-second) vs. energy for rippled waveguide, ($a = 10$ Å).

$\tau = 1 \cdot 10^{-11}$ s at $E = 1.384$ eV and $\tau = 2.8 \cdot 10^{-11}$ s at $E = 1.504$ eV in the integrable waveguide compared to $\tau = 3.21 \cdot 10^{-12}$ s at $E = 1.514$ eV in rippled waveguide. (Note that a classical free electron at these energies would travel the length of the waveguide ($L = 200$ Å) at about 10^{-15} s without making any collision.) A second point to note is that at each energy away from a resonance the chaotic cavity has a longer delay time than the integrable cavity. A third point to note in Figs. 5 and 6 is that for the integrable waveguide the odd modes are uncoupled from the even modes due to the transverse symmetry of the waveguide, whereas in the chaotic waveguide all the modes are coupled together.

The relation between the conductance, G, given by Eq. (6) and the average Wigner delay time, $\langle \tau(E) \rangle = \frac{1}{8} \sum_{n=1}^{8} (d\theta_n/dE)$, is shown in Fig. 7. The integrable case has much sharper resonances than the chaotic case.

In the integrable cavity the current carried by a mode can actually drop to zero, whereas in the chaotic cavity we did not find cases where the current drops to zero because the broader resonances always seem to have some overlap. The average Wigner delay time away from resonance is

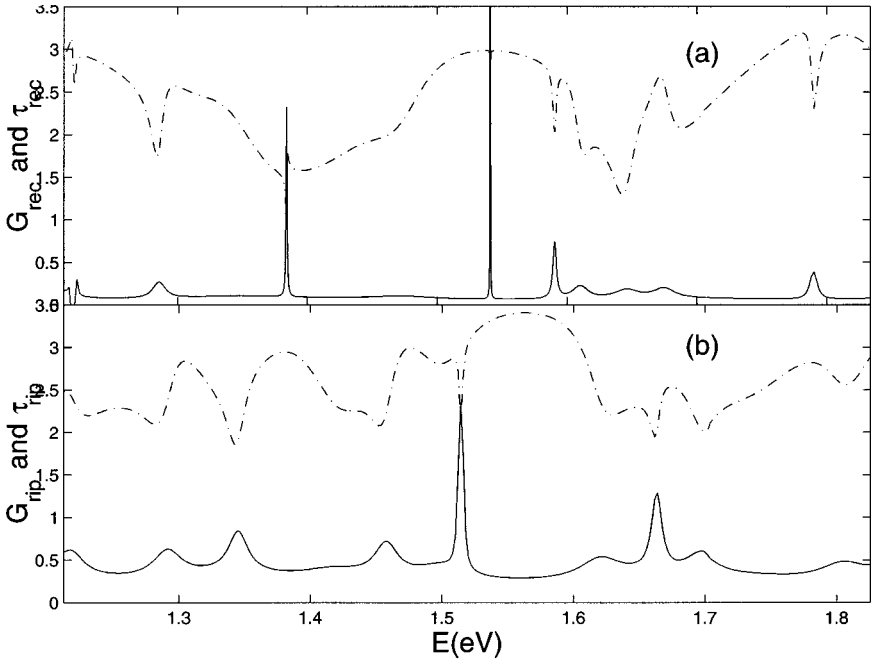

Fig. 7. A comparison of the Landauer conductance, G (dashed lines), with average Wigner delay time (solid line) for (a)integrable cavity, (b) ripple cavity ($a = 10$ Å). G is given in units of conductance quanta, $2e^2/h = 77\,\mu$S and τ is given in units of pico-seconds.

consistently greater for the chaotic cavity than for the integrable cavity primarily because the resonances in the chaotic cavity are broader.

It is useful to look at the auto-correlation function, $C_\tau(\Delta E)$, for the Wigner time delay to determine the energy range over which the delay times are correlated. It is defined

$$C_\tau(\Delta E) \equiv \left(\frac{N}{\pi}\right)^2 \frac{1}{2N(E_2 - E_1)} \sum_n^{2N} \int_{E_1}^{E_2} dE \left[\frac{d\theta_n(E+\Delta E)}{dE} \frac{d\theta_n(E)}{dE} - \left(\frac{d\theta_n(E)}{dE}\right)^2 \right] \tag{12}$$

The auto-correlation functions for each propagating mode are shown in Fig. 8. We averaged $C_\tau(\Delta E)$ over an energy interval, $[E_1 = 1.212\,\text{eV}, E_2 = 1.7\,\text{eV}]$ which supports four propagating modes in the leads. We approximated the integration in Eq. (12) by a summation over 244 energies with spacing 0.002 eV. The correlation function changes its form from a Lorentzian behavior for small ΔE to exponential decay with decreasing

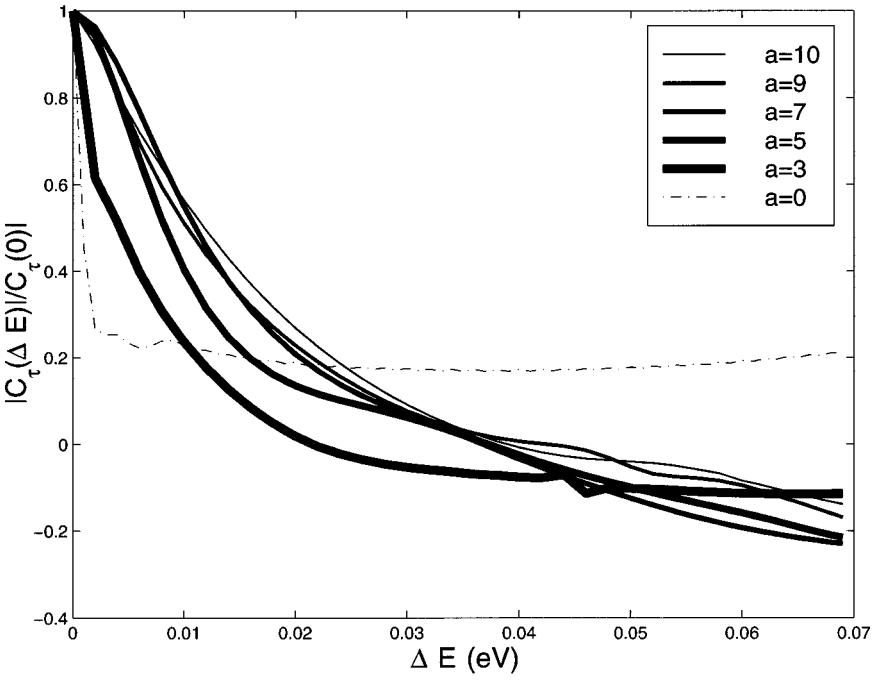

Fig. 8. The auto-correlation function of Wigner delay times (normalized to unity at zero delay) averaged over phases. The dashed line is for the integrable waveguide. Several different ripple sizes are shown.

ripple size. As is the case for the correlation of eigenvalues, the correlation of delay times inside the integrable waveguide falls off faster than in the chaotic waveguide. The fast decay of delay time correlations in the rectangular cavity can be understood in terms of the sharp resonance peaks. In the rippled cavity resonance peaks are quite wide in energy and the correlation decays more slowly.

The electron probability distribution and current inside the waveguide (given in Eqs. (3) and (4)) also show some features which distinguish the integrable and the chaotic systems at near resonance and off resonance regions. In Fig. 9 we show the electron probability density, $\rho(x, y)$, inside the waveguide cavity for both integrable and chaotic waveguides. Figure 9(a) corresponds to mode 1, Fig. 9(b) mode 2, Fig. 9(c) mode 3, and Fig. 9(d) mode 4 of an integrable waveguide near the resonance energy $E = 1.506$ eV. We have transverse symmetry of wave function which makes $\rho(x, y)$ symmetric in this direction. Similarly, Fig. 9(e) corresponds to mode 1, Fig. 9(f) mode 2, Fig. 9(g) mode 3,and,Fig. 9(h) mode 4 of the

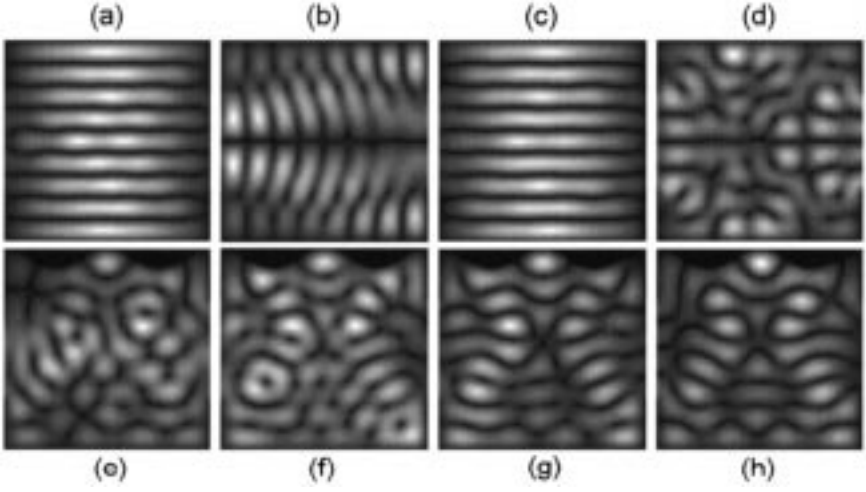

Fig. 9. The charge density for 4 modes of integrable waveguide, at the resonance energy, $E = 1.5406$ eV. Transmission probabilities are (a) $T_1 = 0.532$ (b) $T_2 = 0.561$, (c) $T_3 = 0.247$, and (d) $T_4 = 0.735$. The charge density for 4 modes of the ripple waveguide shown at the resonance energy, $E = 1.514$ eV. Transmission probabilities are (e) $T_1 = 0.880$, (f) $T_2 = 0.265$, (g) $T_3 = 0.463$, and (h) $T_4 = 0.488$.

ripple waveguide ($a = 10$ Å) near the resonance energy $E = 1.514$ eV. The ripple waveguide is not symmetric in the transverse direction, and we don't see transverse symmetry in Figs. 9(e)–(h). We observe that near the resonance energy structures are excited which resemble a superposition of closed system eigenfunctions. Figures 9(a) and 9(c), for example, resemble energy eigenfunction $E_{91} = 1.5416$ eV of the closed billiard, Fig. 9(b) resembles $E_{48} = 1.504$ eV and, Fig. 9(d) resemble $E_{84} = 1.504$ eV which is close to the resonance energy of the open system. This is an indication that these are Fano resonances.[20] From Figs. 9(a) and 9(c) we see that modes 1 and 3 are strongly coupled and have similar probability densities. Note also the similarity of their transmission probabilities (see Fig. 5). For the integrable system, the lack of coupling between the pair of modes 1 and 3 and the pair of modes 2 and 4 is due to the transverse parity of the system. In the rippled waveguide, all the modes are coupled although coupling between mode 3 and 4 is strongest as it can be seen from Figs. 9(g) and 9(h) (see also Fig. 6.).

When multiple modes (channels) flow in the leads, the total current inside the cavity is left-right symmetric. For the integrable case, total current of coupled modes are left-right symmetric. In Fig. 10(a) we show the total current in the rectangular cavity for incident channels 1 and 3 near the resoanance energy, $E = 1.375$ eV. In Fig. 10(b) we show the total

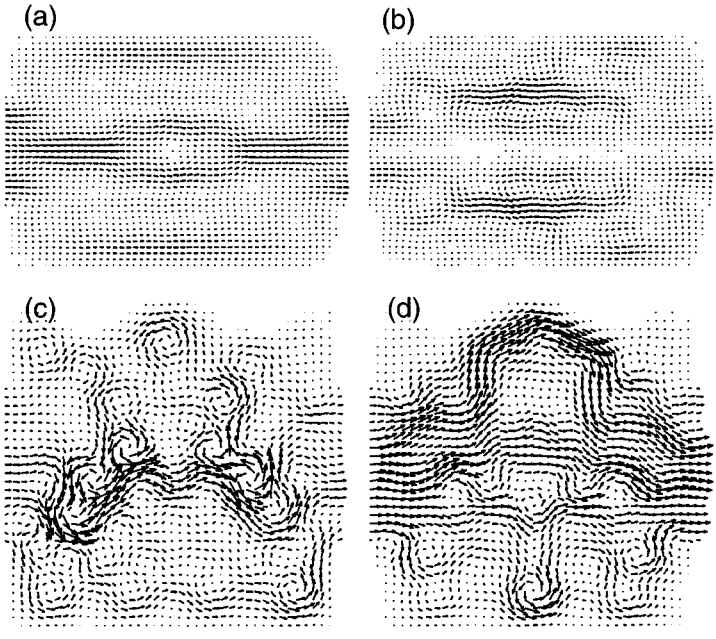

Fig. 10. (a) The sum of the current of mode 1 and mode 3 at resonance, $E = 1.375$ eV for the integrable waveguide. (b) The total current of modes 2 and 4 at resonance, $E = 1.375$ eV for the integrable waveguide. (c) The total current of all 4 modes at resonance energy $E = 1.514$ eV for the chaotic waveguide. (d) Same as (c) but at an off resonance energy, $E = 1.504$ eV.

current inside the rectangular cavity for channels 2 and 4 near resonance energy $E = 1.375$ eV. In Fig. 10(c) we show the total current in the rippled cavity near resonance energy, $E = 1.516$ eV. Figure 10(d) shows the same sum of currents in the chaotic cavity, but at an off resonance energy, $E = 1.504$ eV.

3.2. Comparison to Random Matrix Theory Results

One of the main purposes of this paper is to compare the statistical properties of the S-matrix for the chaotic cavity with the predictions of random matrix theory. The predictions of random matrix theory (RMT) are based on a picture of conductance through a scattering region with the scattering process governed by a random Hamiltonian. In the RMT approach, the scattering problem is often formulated in terms of a model Hamiltonian which involves the coupling of a closed system to the continuum.[18, 21, 17]

(It can also be formulated starting from a random S-matrix.[24]) The model Hamiltonian is,

$$\bar{H} = \sum_{k=1}^{N} E_k |k\rangle\langle k| + \sum_{k=1}^{2N} \int dE\, E\, |c, E\rangle\langle c, E| + g \sum_{c=1}^{2N} \sum_{k=1}^{N} \int dE\, W_{kc}(E)(|k\rangle\langle c, E| + |c, E\rangle\langle k|) \tag{13}$$

where g is the overall strength of the coupling between the continuum (the leads) and the scattering region (the cavity), and $W_{kc}(E)$ gives the strength of this coupling as a function of energy. The Hilbert space is spanned by N discrete states $|k\rangle$ (eigenstates of the closed cavity) and $2N$ continuum states, $|c, E\rangle$ (channels in the leads). If W depends weakly on energy, then the S-matrix is given by,

$$S(\bar{E}) = \frac{1 + i\bar{K}}{1 - i\bar{K}}, \qquad \bar{K} = g^2 W^{\dagger} \frac{1}{E - \bar{H}_{\text{eff}}} W \tag{14}$$

where $H_{\text{eff},\,kl} = H_{kl} - ig^2 \sum_{c=1}^{2N} W_{kc} W_{cl}$ is the effective Hamiltonian. One prediction of RMT[18] is that near a resonance, the Wigner delay time, $\tau_n(E)$, can be written

$$\tau_n = \frac{\Gamma_n}{(E - E_n)^2 + \Gamma_n^2/4} \tag{15}$$

where E_n is the resonance energy and Γ_n is the resonance width. In ref. 21, eigenvalues and eigenvectors of the auxiliary matrix, $\bar{K}$, have been used to find the distribution of partial delay times, $P(\tau_n)$. Their result for arbitrary coupling strength g is,

$$P(\tau_n) = \frac{e^{(-g^2/\tau_n)}\, {}_1F_1(N; N + 1/2; (g^2 - g^{-2})/\tau_n)}{g^{(2N-1)}\Gamma(N + 1/2)\, \tau_n^{(N+3/2)}} \tag{16}$$

where we have written $P(\tau_n)$ for a Gaussian Orthogonal Ensemble(GOE). The function, ${}_1F_1(a, b, z)$, is the confluent hypergeometric function. N is the number of propagating modes (channels) in the leads.

We have compared our results with predictions of random matrix theory. We have four modes in the leads so we take $N = 4$ in Eq. (16). We have constructed of histogram of 10808 values of the Wigner delay time taking delay times for five different ripple amplitudes, $a = 3, 5, 7, 9, 10$ Å, in order to improve our statistics (Fig. 11). The distribution in Eq. (16)

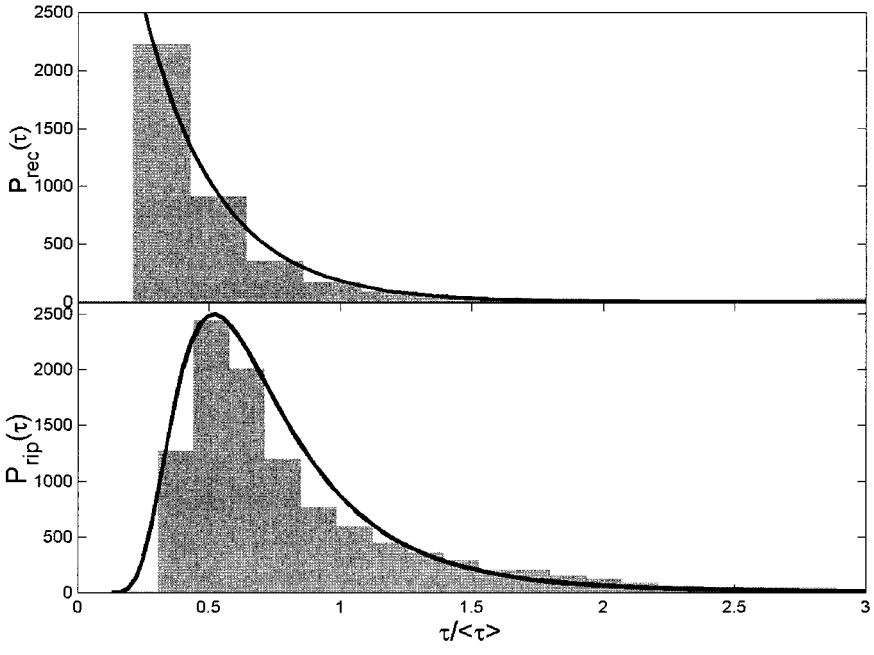

Fig. 11. Histogram of Wigner delay times for (a) integrable and (b) ripple waveguides. In case (a), there are a total of 4120 data points. This data can be described in terms of a Poisson distribution.The fitted curve is $\exp(-\tau/<\tau)$. In case (b), a total of 10808 data points is used. The fitted curve is from Eq. (16) using $P(\tau)=\sum_{n=1}^{8} P(\tau_n)$.

shows good agreement with our numerical data (see Fig. 9b) for the coupling strength $g=2.3$. This value of g indicates a strong coupling between channels in the leads and the eigenmodes of the cavity. This is not unexpected since we have a rather large ratio of the width of leads to the cavity width. The integrable channel results cannot be described with RMT. If we compare the distribution of delay times for the integrable (Fig. 9a) and chaotic cases (Fig. 9b), we again see the systematically longer delay times in the chaotic cavity.

The correlation function for S-matrix elements in RMT has been found for the GOE case in ref. 28. They used an ensemble average of matrix elements and assumed ergodicity to compare their results with the more conventional energy averaged case. In ref. 17 it is shown that the diagonalized S-matrix should have the same statistical properties as the undiagonalized case. Since in our system leads are aligned, this correlation function shows oscillatory behavior for larger values of ΔE. There is no explicit expression for $C_\tau(\Delta E)$, but in ref. 26 limiting values have been obtained. For small ΔE RMT predicts that it should behave like a

Lorentzian and for large ΔE it asymptotically approaches $-2/(\pi \Delta E)^2$ for the chaotic waveguide (see, for example, refs. 26 and 27) which is in agreement with Fig. 8.

We have also calculated the distribution the widths of delay time resonance peaks. To build statistics we again used different ripple sizes, $a = 3, 5, 7, 9, 10$ Å. The first and second derivatives of partial time delays were used to find the delay times at resonance energies and their full width at half maximum (FWHM). While calculating FWHM, we used inflection points (roots of second derivatives) to find the height of resonance delay times when they were comparable to the average delay time. The distribution of widths for a chaotic system is predicted to be a χ^2 distribution when coupling to the continuum is weak. When coupling to the continuum is strong the distribution is changed to power law decay.[25] We observed a $\Gamma^{-3/2}$ dependence of the scaled widths in our system (see Fig. 12). We also observed that for the integrable case we have what appears to be an exponential decay of the distribution.

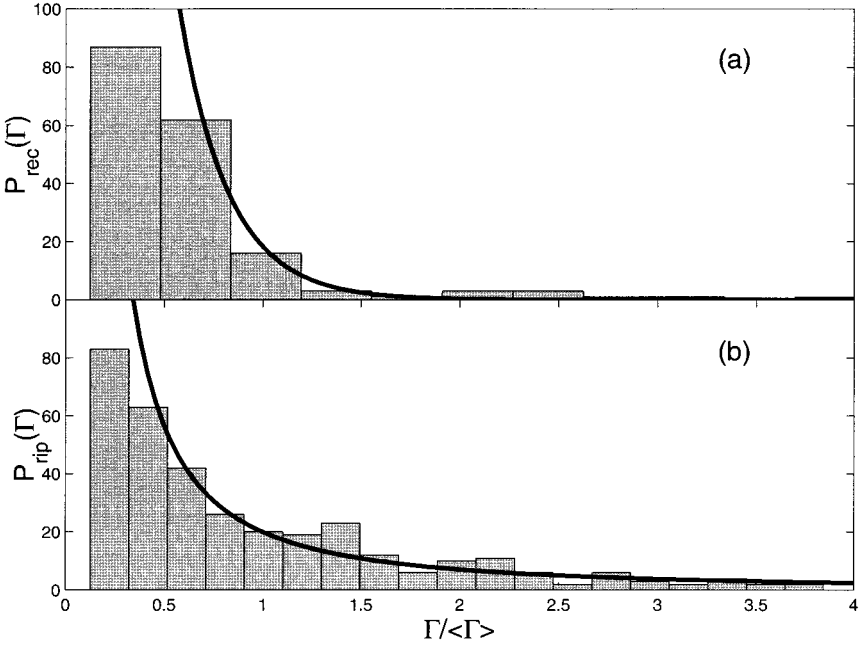

Fig. 12. The distribution of resonance widths for (a) integrable and (b) ripple waveguides. In (a) we used 185 resonances and fitted the histogram to the function, $\exp(-4\Gamma/\langle\Gamma\rangle)$. In case (b) we have 350 resonances and we have fitted the histogram with the function, $(\Gamma/\langle\Gamma\rangle)^{-3/2}$.

4. CONCLUDING REMARKS

Our numerical results indicate that the behavior of ballistic electron waves in the waveguide depends strongly on geometry. Classically chaotic geometries produce characteristically different transport properties than integrable geometries. The electron suffers systematically longer delays when traversing the chaotic cavity than when traversing the integrable cavity. We have examined transport properties in several ways. We have determined the energy dependence of transmission probabilities, Wigner delay times, S-matrix eigenvalue correlations, and Wigner delay time correlations. We have determined the spatial dependence of probability densities and current distributions at resonance energies. We found differences in resonance structures in the chaotic and integrable geometries.

The statistical distribution of eigenvalue spacings in a closed system provides a signature of quantum chaos as we have seen for the closed counter part of our system. In random matrix theories and semi classical calculations it was found that the chaotic behavior of an underlying closed system directly affects the properties of the system when it is open. We confirm this for our system by calculating the S-matrix for our chaotic open system directly. We see that Wigner delay times derived from the S-matrix have different distributions in integrable and chaotic wave guides. We compared the distribution for the chaotic case with random matrix theory predictions and we found good agreement with those predictions. The distribution of resonant delay time widths also shows characteristic differences for integrable and chaotic geometries.

APPENDIX

In this Appendix, we show how to diagonalize the Hamiltonian matrix for the closed rippled box. After the coordinate change,

$$u = x, \qquad v = \frac{y}{b + a \cdot \cos((4\pi/L)\, x)} \tag{17}$$

we have a differential equation defined in a rectangular region with coordinates, (u, v). The Schrödinger equation in terms of the coordinates, u and v, is given by

$$-\frac{h^2}{2m}\left(\partial_u^2 + h_1 \partial_v^2 + h_2 \partial_{uv}^2 + h_3 \partial_v\right) \psi_l(u, v) = E_l \psi_l(u, v) \tag{18}$$

with boundary conditions $\psi_l(0, v) = 0$, $\psi_l(200, v) = 0$, $\psi_l(u, 0) = 0$, and $\psi_l(u, 1) = 0$. Note that the wave function is normalized as

$$\iint \sqrt{g}\, \psi_l^\dagger(u, v)\, \psi_{l'}(u, v)\, du\, dv = \delta_{ll'} \tag{19}$$

where g is defined such that $g^{-1/4} = [b + a \cdot \cos((4\pi/L) \cdot x)]^{-1/2}$.

The solution, $\psi_l(x, y)$, can be expanded in terms of a Fourier basis,

$$\psi_l(u, v) = \sum_{m=1}^{\infty} \sum_{n=1}^{\infty} B_{mn}^l \phi_{mn}(u, v) \tag{20}$$

with

$$\phi_{mn}(u, v) = \pi^{-1/2} g^{-1/4} \sin(m\pi v) \sin(n\pi u/L) \tag{21}$$

where B_{mn}^l are the unknown expansion coefficients. As a result of this expansion, the boundary value problem can be transformed into the eigenvalue problem,

$$\sum_{m=1}^{\infty} \sum_{n=1}^{\infty} H_{mnm'n'} B_{mn}^l = E_l B_{mn}^l \tag{22}$$

The Hamiltonian matrix elements, $H_{mnm'n'}$, are given by

$$H_{mnm'n'} = \int_0^L du \int_0^1 dv\, \partial_\alpha(\sin(m\pi v) \cdot f^\dagger) \cdot P \cdot g^{\alpha\beta} \cdot \partial_\beta(\sin(m'\pi v) \cdot f') \tag{23}$$

where $f \equiv \sin(n\pi u/L)/\sqrt{P} = f^\dagger$, $f' \equiv \sin(n'\pi u/L)/\sqrt{P} = f'^\dagger$, $P \equiv b + a \cdot \cos((4\pi/L)\, x)$, and $g^{\alpha\beta}$ is the (α, β) matrix element of the metric matrix,

$$\bar{g} \equiv \begin{pmatrix} 1 & \dfrac{4\pi \cdot a \cdot v \cdot \sin(4\pi u/L)}{L \cdot P} \\ \dfrac{4\pi \cdot a \cdot v \cdot \sin(4\pi u/L)}{L \cdot P} & \dfrac{L^2 + 4\pi \cdot a \cdot v \cdot \sin(4\pi u/L)^2}{L^2 \cdot P^2} \end{pmatrix}$$

We calculate the Hamiltonian matrix element using Eq. (23). We reduce the double integral to a single integral after integrating in the v

direction. After some algebra we find the following form which is suitable for numerical calculations,

$$H_{mnm'n'} = \frac{n^2\pi^2\delta_{nn'}\delta_{mm'}}{4L} + 2\pi^2 a^2 J^4_{nn'}\delta_{mm'} + \frac{8a^2m^2\pi^4}{3L^2} J^4_{nn'}\delta_{mm'}$$
$$+ (1-\delta_{mm'})\, K_1 \cdot \frac{4\pi}{L}\, a(nJ^2_{nn'} - n'J^2_{n'n}) + (1-\delta_{mm'})\, K_2 J^4_{nn'}\, \frac{16\pi^2}{L^2}\, a^2 \tag{24}$$

where $K_1 \equiv (4/\pi^2)[mm'/(m^2-m'^2)]$, $K_2 \equiv [mm' \cdot (\pi^2 m'^4 - 12m'^2 - 2mm'^2\pi^2 + m^4\pi^2 - 4m^2)]/\pi^2(m-m')^3\,(m+m')^3$ and the integrals are defined as,

$$J^2_{nn'} \equiv \int_0^L du\, \sin(n\pi u/L)\cos(n'\pi u/L)\sin(4\pi u/L)/P,$$

$$J^3_{nn'} \equiv \int_0^L du\, \sin(n\pi u/L)\sin(n'\pi u/L)/P,$$

$$J^4_{nn'} \equiv \int_0^L du\, \sin(n\pi u/L)\sin(n'\pi u/L)\sin^2(4\pi u/L)/P^2,$$

$$J^5_{nn'} \equiv \int_0^L du\, \sin(n\pi u/L)\sin(n'\pi u/L)\sin(4\pi u/L)/P$$

The eigenvalues and eigenvectors of H can be calculated efficiently due to the sinusoidal integrals. Eigenvectors of H give values for the expansion coefficients, B^l_{mn}, and the eigenfunctions in u-v space can be found from these coefficients. The solution can then be transformed back to x-y space to see the wave-function in real space.

5. ACKNOWLEDGEMENTS

The authors wish to thank the Robert A. Welch Foundation Grant No. F-1051, NSF Grant No. INT-9602971, and DOE Contract No. DE-FG03-94ER14405 for partial support of this work. We thank NPACI and the University of Texas at Austin High Performance Computing Center for use of their computer facilities. The authors also wish to thank Kyungsun Na, Suhan Ree, C. H. Lewenkopf, H. U. Baranger, R. A. Jalabert, and P. A. Mello for helpful discussions. LER wishes to thank the Aspen Center for Physics for their kind hospitality.

REFERENCES

1. C. M. Marcus, R. M. Wesrevelt, P. f. Hopkins, and A. C. Gossard, *Chaos* **3**(4):643 (1993); I. H. Chan, R. M. Clarke, C. M. Marcus, K. Campman, and A. C. Gossard, *Phys. Rev. Lett.* **74**:3876 (1995); A. G. Huibers, S. R. Patel, C. M. Marcus, P. W. Brouwer, C. I. Duruoz, and J. S. Harris, Jr., *Phys. Rev. Lett.* **81**:1917 (1998).
2. A. M. Chang, H. U. Baranger, L. N. Pfeiffer, and K. W. West, *Phys. Rev. Lett.* **73**:2111 (1994); C. M. Marcus *et al.*, *Surf. Sci.* **305**:480 (1994).
3. L. E. Reichl, *The Transition to Chaos In Conservative Classical System: Quantum Manifestations*, first edition (Springer-Verlag, 1992).
4. W. A. Lin, J. B. Delos, and R. V. Jensen, *Chaos* **3**(4):655 (1993).
5. Harold U. Baranger, Rodolfo A. Jalabert, A. Douglas Stone, *Chaos* **3**(4):665 (1993).
6. Pier A. Mello, *Physique Quantique Mesoscopique* (Elsevier Science, 1995), p. 435.
7. C. W. J. Beenakker, *Rev. Modern Phys.* **69**(3):731 (1997).
8. Thomas Guhr, Axel Muller-Groeling, and Hans A. Weidenmuller, *Phys. Rep.* **299**:190 (1998).
9. C. Rouvines and U. Smilansky, *J. Phys. A* **28**:77 (1994).
10. Eyal Doron and U. Smilansky, *Nonlinearity* **5**:1055 (1991).
11. G. A. Luna-Acosta, Kyungsan Na, L. E. Reichl, and A. Krokhin, *Phys. Rev. E* **53**(4): 3271 (1996).
12. Freeman J. Dyson, *J. Math. Phys.* **3**(1):140 (1961).
13. Klaus-Jurgen Bathe, *Finite Element Procedures*, first edition (Prentice–Hall, 1996), Chapters 10 and 11.
14. Harold U. Baranger and Pier A. Mello, *Phys. Rev. B* **54**(20):14297 (1996).
15. Craig S. Lent and David J. Kirkner, *J. Appl. Phys.* **67**(10):6353–6359 (1990); David J. Kirkner, Craig S. Lent, and Sirinavas Sivaprakasam, *International Journal of Numerical Methods in Engineering* **29**:1527 (1990).
16. Yongjiang Wang, Ningjia Zhu, Jian Wang, and Hong Guo, *Phys. Rev. E* **54**(3):2438 (1996).
17. C. H. Lewenkopf and H. A. Weidenmuller, *Ann. Phys.* **212**:53 (1991).
18. Yan V. Fyodorov and Hans-Jurgen Sommers, *J. Math. Phys.* **38**(4):1918 (1997).
19. Wolfgang Porod, Zhi-an Shao, and Craig S. Lent, *Phys. Rev. B* **48**:8495 (1993).
20. Erkan Tekman and Philip F. Bagwell, *Phys. Rev. B* **48**(4):2553 (1993).
21. Petr Seba, Karol Zyczkowski, and Jakub Zakrzewski, *Phys. Rev. E* **54**(3):2438–2445 (1996).
22. E. Haller, H. Koppel, and L. S. Cederbaum, *Chem. Phys. Lett.* **101**:215 (1983).
23. P. W. Brouwer, K. M. Frahm, and C. W. J. Beenakker, *Phys. Rev. Lett.* **78**(25):4737 (1997).
24. P. A. Mello and H. U. Baranger, *Waves in Random Media* **9**:105 (1999).
25. T. Gorin, F.-M. Dittes, M. Muller, I. Rotter, and T. H. Seligman, *Phys. Rev. E* **56**(3):2481 (1997).
26. Eduardo R. Mucciolo, Rodolfo A. Jalabert, and Jean-Louis Pichard *J. Phys. I* **7**:1297 (1997).
27. Bruno Eckhardt, *Chaos* **3**(4):613 (1993).
28. J. J. M. Verbaarschot, H. A. Weidenmuller, and M. R. Zirnbauer, *Phys. Rep.* **129**:367 (1985).